Proceedings of the 11th Brazilian Congress of Thermal Sciences and Engineering – ENCIT 2006
Braz. Soc. of Mechanical Sciences and Engineering – ABCM, Curitiba, Brazil, Dec. 5-8, 2006

Paper CIT06-950

A Numerical Study of Turbulent Wake Flow Behind a Finite Cylinder

Luciano G. Noleto
Universidade de Brasília. Departamento de Engenharia Mecânica, LEA - Laboratório de Energia e Ambiente. 70910-900 Brasília. DF. Brazil.
lucianonoleto@unb.br

Antonio C. P. Brasil Junior
Universidade de Brasília. Departamento de Engenharia Mecânica, LEA - Laboratório de Energia e Ambiente. 70910-900 Brasília. DF. Brazil.
brasiljr@unb.br

Abstract. *In this work a numerical study concerning the turbulent flow over a finite cylinder attached on a flat plate is presented. The flow is simulated using three different methodologies: Unsteady Reynolds Averaged Navier Stokes equations (URANS), Detached Eddy Simulation (DES) and Large Eddy Simulation (LES). The results of the simulation have been used to study the turbulence characteristics in the wake flow behind the cylinder, and the interactions between the great structures of the unsteady flow, with the fine turbulence. Numerical simulations were performed with a finite volume method with unstructured tetrahedral meshes, which can promote a most adequate discretization for this kind of flow. The URANS and DES simulations were performed using SST model. This model is used for closuring of the averaged equation, and also as a subgrid model for the DES approach. The results show the average flow for the three methodologies, as well as velocity profiles compared with experimental results.*

keywords: *Large Eddy Simulation, Detached Eddy Simulation, URANS, Finite Cylinder, Vortex formation*

1. Introduction

The flow around a circular cylinder has several applications. One of them is at canopy flows, where the cylinder can represent an obstacle, being this obstacle one or several trees in a forest or buildings in a major city. The immediate engineering application is at fluid structure interaction. This happens at flows under bridges, oil platforms and buildings. The circular cylinder can be represented by a bluff body that shows 3-Dimensional altered flow characteristics in the axial direction. It is caused by the non-uniformity of free stream flow, longitudinal vortices and low aspect ratio of the cylinder. The flow pattern is a horseshoe vortex close to the wall that the cylinder is mounted, and depending of the flow characteristics, a vortex shedding is developed downstream, with a 3-Dimensional separated flow at the free end surface. The shedding is linked to the aspect ratio of the cylinder. The fact of the cylinder being finite influences the topology of the flow. The use of modern tools for numerical simulation of this kind of flow allows the capture of several turbulent phenomena inherent to the flow. Between those tools, there are large eddy simulation and, more recently, detached eddy simulation (Noleto and Brasil-Junior, 2005).

DES was tested in several cases of Large Eddy Simulation (LES), to check the reliability of the model for engineering cases. Constantinescu and Squires, 2003, investigated the flow over a sphere in super critical regime with LES and DES. The authors had concluded that the DES model accurately predict massively separated flows and it was able to predict also the large scale shedding of hairpin-like structures and the formation of Kelvin-Helmholtz instabilities. Squires *et al.*, 2002, made a analysis of massive separated flows in aircrafts using DES, concluding that the prediction of lift and drag are accurate in comparison with flight data, and also predicts with accuracy the pressure in the supersonic flow over the aircraft. The work of Forsythe *et al.*, 2001, is the use of detached eddy simulation to predict the flow over a forebody cross section, concluding that the predictions of the model are robust, with little differences between experimental data and the simulation. Frohlich and Rudi, 2004, made a numerical study of the flow past a finite cylinder using LES. The authors chose a cylinder aspect ratio of 2.5 in order to capture some vortex shedding. First, the results were analyzed in the light of subgrid modeling. With coarse grids, the dynamic model show deficient results when compared with the Smagorinsky model. Then the results were analysed in the light of physics, showing the existence of tip and arch vorticity in the average flow. Kanda *et al.*, 2004, performed LES at a simple cube array in order to study urban canopy flow. A comparison with experimental results is showed. Their results are analyzed using spatial and time averaging. It shows the presence of canyon-type flows between the cubes. The recirculation within the canopy had influenced the turbulent statistics.

Concerning to finite cylinder flows, there is the confirmation of the presence of a pair of vortices around the free end surface from iso-velocity lines in the wake near the tip region and this work identified this pair of vortices as trailing side tip vortices (Kawamura *et al.*, 1984). There is also a work (Baban *et al.*, 1989) who observed an increase in drag force fluctuations due to highly turbulent recirculation flow in the wake region, especially in the shear layer separated from the end of the cylinder. A visualization of the flow over the free end surface of a finite cylinder mounted on a flat plate using oil-streak line methods and smoke-laser. Roh and Park, 2003, showed that the flow at the free end surface is topologically characterized by two spiral nodes and a separation saddle point in the front portion and two attachment nodes and a separation saddle point in the rear part. A study of the free end effects in finite cylinder flows (Park and Lee, 2000) observed that the vortex shedding frequency decreases and the the vortex formation region increases as the aspect ratio decreases. The vortex formation region and periodic vortex shedding disappear very close to the free end. A experimental study of a small forest model based on a single cylinder and a cylinder matrix (Cala, 1996) in wind tunnel obtained profiles who holds great resemblance with similar work.

This paper will show results of the numerical simulation of a circular cylinder mounted in a flat plate with ANSYS-CFX commercial software. The used formulations were large eddy simulation, detached eddy simulation and URANS. The chosen case is the single cylinder studied by Cala, 1996.

2. Mathematical Modeling

2.1. Large Eddy Simulation

The large eddy simulation modeling uses a spatial averaging. The aim is to separate the small eddy from the large eddy. The large eddy is solved directly, and the small eddy is modeled using a subgrid model (Silveira-Neto, 2002, Lesieur and Métais, 1996, Silvestrini, 2003). The Navier-Stokes equations are given as follows:

$$\frac{\partial u_i}{\partial x_i} = 0 \tag{1}$$

$$\frac{\partial u_i}{\partial t} + \frac{\partial (u_i u_j)}{\partial x_j} = -\frac{1}{\rho}\frac{\partial p}{\partial x_i} + \nu \left[\frac{\partial}{\partial x_j} \left(\frac{\partial u_i}{\partial x_j} + \frac{\partial u_j}{\partial x_i} \right) \right] \tag{2}$$

u is the velocity, p is the pressure and ν is the kinematic viscosity. The separation of the eddies is performed as follows, for any given variable of the flow f:

$$f = \overline{f} + f' \tag{3}$$

The large eddy part $\overline{f}$ can be written as:

$$\overline{f}(x_i, t) = \int_V G(x_i - x_i') f(x_i, t) dx_i' \tag{4}$$

$G(x_i - x_i')$ is the tophat filter, written as follows:

$$G(x_i) = \begin{cases} \frac{1}{\Delta^3}; & \text{se } |x_i| \leq \frac{\Delta}{2} \\ 0; & \text{se } |x_i| > \frac{\Delta}{2} \end{cases} \tag{5}$$

Δ is the characteristic size of the filter. The filtered Navier-Stokes equations are given as follows:

$$\frac{\partial \overline{u}_i}{\partial x_i} = 0 \tag{6}$$

$$\frac{\partial \overline{u_i}}{\partial t} + \frac{\partial \overline{u_i u_j}}{\partial x_j} = -\frac{1}{\rho}\frac{\partial \overline{p}}{\partial x_i} + \nu \left[\frac{\partial}{\partial x_j} \left(\frac{\partial \overline{u}_i}{\partial x_j} + \frac{\partial \overline{u}_j}{\partial x_i} \right) \right] \tag{7}$$

Developing the convective part of equation 7 with equation 3 yields to:

$$\overline{u_i u_j} = \overline{u}_i \overline{u}_j + \overline{\overline{u_i} u_j'} + \overline{\overline{u_j} u_i'} + \overline{u_i' u_j'} + L_{ij} \tag{8}$$

Using 8 yields the filtered Navier-Stokes equations to:

$$\frac{\partial \overline{u}_i}{\partial t} + \frac{\partial \overline{u_i u_j}}{\partial x_j} = -\frac{1}{\rho}\frac{\partial p}{\partial x_i} + \frac{\partial}{\partial x_j} \left[\nu \frac{\partial \overline{u}_i}{\partial x_j} - (\tau_{ij} + C_{ij} + L_{ij}) \right] \tag{9}$$

$$\frac{\partial \overline{u}_i}{\partial x_i} = 0 \tag{10}$$

Where:

- $L_{ij} = \overline{\overline{u}_i \overline{u}_j} + \overline{\overline{u}_i u_j'}$ - Leonard tensor
- $C_{ij} = \overline{\overline{u}_j u_i'} + \overline{u_i' u_j'}$ - Crossed terms
- $\tau_{ij} = \overline{u_i' u_j'}$ - Subgrid Reynolds tensor

2.1.1. Smagorinsky Subgrid Model

The subgrid Reynolds tensor is modeled using the Boussinesq eddy viscosity (ν_t) assumption:

$$\tau_{ij} = \nu_t \left(\frac{\partial \overline{u_i}}{\partial x_j} + \frac{\partial \overline{u_j}}{\partial x_i} \right) - \frac{2}{3} k \delta_{ij} \tag{11}$$

The production ($\wp$) is denoted as a function of the shear rate and the dissipation (ε) is denoted as a function of the velocity and of the subgrid characteristic length:

$$\wp = 2\nu_t S_{ij} S_{ij} \tag{12}$$

$$\varepsilon = \frac{-c_1 (\overline{u_i' u_j'})^{1,5}}{\ell} \tag{13}$$

The velocity scale is related with the filtered velocity gradients by an analogy of the Prandtl mixing length. So, with scaling and the production and dissipation equations, the eddy viscosity can be written as follows:

$$\nu_t = (C_s \ell)^2 \sqrt{2 S_{ij} S_{ij}} \tag{14}$$

Here, C_s is the Smagorinsky constant and S_{ij} is the rate-of-strain tensor. The value of the Smagorinsky constant for the present work is equal to 0,2.

2.1.2. Wall Damping

To avoid high values of the eddy viscosity, a wall damping function is used. The damping is made using a combination of the mixing length and a damping function for the eddy viscosity:

$$\nu_t = min(l_{mix}, f_\nu C_s \Delta)^2 \sqrt{2 S_{ij} S_{ij}} \tag{15}$$

Here, f_ν is the damping function, C_s is the Smagorinsky constant and S_{ij} is the rate-of-strain tensor. The mixing length is given as follows:

$$l_{mix} = K y_{wall} \tag{16}$$

The default value of the Smagorinsky constant and the K constant is 0,1 e 0,4 respectively. The damping function used at the present work is the Piomelli function (Rudman and Blackburn, 1999), given by:

$$f_\nu = \sqrt{1 - exp\left[\left(\frac{-\widetilde{y}}{A} \right)^3 \right]} \tag{17}$$

A is the damping factor, equal to 25. The normalized wall distance is given by:

$$\widetilde{y} = \frac{y \widetilde{u}}{\nu} \tag{18}$$

2.2. Reynolds Averaging - The SST Model

In a frame work for turbulence modeling, for incompressible turbulent flows, the conservation of mass, and momentum (equations 1 and 2) can be expressed by the classical Reynolds averaged equations given by:

$$\frac{\partial u_i}{\partial x_i} = 0 \tag{19}$$

$$\rho \left(\frac{\partial u_i}{\partial t} + u_j \frac{\partial u_i}{\partial x_j} \right) = -\frac{\partial p}{\partial x_i} + \frac{\partial}{\partial x_i} \left[(\mu + \mu_t) \frac{\partial u_i}{\partial x_j} \right] \tag{20}$$

In those equations u_i and p are the mean velocity and pressure fields. Menter (Menter and Kuntz, 2003) created the SST model, and its principle lies on blending the $k - \epsilon$ and the $k - \omega$ model. Far from the wall, the model uses the $k - \epsilon$ formulation, and near the wall, the model uses the $k - \omega$ model. The turbulent eddy viscosity is defined by:

$$\nu_t = \frac{a_1 k}{\max(a_1 \omega, S F_2)} \tag{21}$$

The transport equations are:

$$\rho\left(\frac{\partial k}{\partial t}+u_i\frac{\partial k}{\partial x_i}\right)=P_k-\beta' k\omega\rho+\frac{\partial}{\partial x_i}\left[(\mu+\frac{\mu_t}{\sigma_k})\frac{\partial k}{\partial x_i}\right] \tag{22}$$

$$\rho\left(\frac{\partial \omega}{\partial t}+u_i\frac{\partial \omega}{\partial x_i}\right)=\alpha\rho S^2+\beta\rho\omega+\frac{\partial}{\partial x_i}\left[(\mu+\frac{\mu_t}{\sigma_\omega})\frac{\partial \omega}{\partial x_i}\right]+2(1-F_1)\rho\sigma_{\omega 2}+\frac{1}{\omega}\frac{\partial k}{\partial x_i}\frac{\partial \omega}{\partial x_i} \tag{23}$$

S is an invariant measure of the rate-of-strain tensor S_{ij} and F_2 is one of two blending functions of the model. The formulation of the blending functions F_1 and F_2 are based on the distance of proximity of the surface and on the flow's variables. The blending functions F_1 and F_2 are given as follows:

$$F_1=\tanh(\arg_1^4) \tag{24}$$

$$\arg_1=\min\left[\max\left(\frac{\sqrt{k}}{\beta'\omega},\frac{500\nu}{y^2\omega}\right),\frac{4\rho\sigma_{\omega 2}k}{CD_{k\omega}y^2}\right] \tag{25}$$

$$CD_{k\omega}=\max(2\rho\sigma_{\omega 2}\frac{1}{\omega}\nabla k\nabla\omega,1,0.10^{-10}) \tag{26}$$

Here, y is the distance to the wall. F_1 is equal to zero away from the surface ($k-\epsilon$ model), and switches over to 1 inside the boundary layer ($k-\omega$ model). F_2 is given by:

$$F_2=\tanh(\arg_2^2) \tag{27}$$

$$arg_2=\max\left(\frac{2\sqrt{k}}{\beta'\omega y},\frac{500\nu}{y^2\omega}\right) \tag{28}$$

F_2 restrains the limitator for the boundary layer wall. A production limiter is used to avoid the growth of turbulence in stagnation regions:

$$P_k=\mu_t\frac{\partial U_i}{\partial x_j}\left(\frac{\partial U_i}{\partial x_j}+\frac{\partial U_j}{\partial x_i}\right) \tag{29}$$

$$\widetilde{P_k}=max(P_k,10\cdot\rho\beta^*k\omega) \tag{30}$$

The model's constants are accounted by a blend of the corresponding constants of the $k-\epsilon$ and $k-\omega$ models with the following function:

$$\alpha=\alpha_1F+\alpha_2(1-F)+... \tag{31}$$

The constants are β'=0.09, α_1=5/9, β_1=3/40, σ_{k1}=0.5, $\sigma_{\omega 1}$=0.5, α_2=0.44, β_2=0.0828, σ_{k2}=1, $\sigma_{\omega 2}$=0.856. The analytical expression for ω provided by ω-equation turbulence models allows a near-wall formulation, which gradually switches from wall-functions to low-Re near wall formulations. At the same time, the mesh is refined in wall normal direction.

2.3. Detached Eddy Simulation

The DES model is a hybridization of a LES approach (Spalart, 2000). DES takes advantage of the RANS method where the mean flow remains attached and steady while offering, like LES, the sensitivity to capture, for instance, wakes or recirculation zones. There are two issues in this approach:

- How fast the turbulent structures will develop after the formulation change to RANS from LES?
- How the changing formulation mechanism must be modeled, in order to avoid a grid induced separation?

The answer lies in the blending functions of the SST model. These functions will "shield" the boundary layer and minimize the grid-induced separation. The formulation change will happen when the turbulent length scale obtained in the RANS section of the model surpasses the local grid spacing. The modeling of the DES SST model uses the SST model and the switching modeling, given as follows:

$$\varepsilon=k\beta'\omega=\frac{k^{\frac{3}{2}}}{L_t}\Rightarrow\frac{k^{\frac{3}{2}}}{C_{DES}\Delta} \tag{32}$$

For $C_{DES}\Delta < L_t$:

$$\Delta = max(\Delta_i); L_t = \frac{\sqrt{k}}{\beta'\omega} \tag{33}$$

Here, the switch from the SST model to an LES formulation is made only in regions where the turbulent length, L_t, predicted by the RANS model is larger than the local grid spacing. Strelets, 2001 propose the following modification to the model, formulated as a multiplier of the destruction term in the turbulent kinetic energy:

$$\varepsilon = k\beta'\omega \Rightarrow k\beta'\omega F_{DES}; F_{DES} = max(\frac{L_t}{C_{DES}\Delta}, 1) \tag{34}$$

Here, $C_{DES} = 0,61$ is the limiter who should be active in the RANS region, specifically in the $k-\epsilon$ region. The numerical formulation is also switched from an upwind biased in the RANS region and a central difference scheme in the DES region. The third blending function is modeled in CFX as follows:

$$F_{DES-SST} = max(\frac{L_t}{C_{DES}\Delta}(1 - F_{SST}), 1) \tag{35}$$

Putting $F_{SST} = 0$ recovers the Strelets formulation. F_2, showed before, shields more of the boundary layer and is therefore the desired default. However, even F_2 does eliminate the problem, but reduces it by an order of magnitude. The set-up of the DES SST model was set according with the work of Menter and Kuntz, 2003.

3. Computational Details and Boundary Conditions

For inflow surfaces the values of velocity, kinetic energy of turbulence and dissipation fields are prescribed. For outflow boundaries, the homogeneous Neumann conditions are prescribed for the same variables and the homogeneous Dirichlet boundary condition is used for the pressure field.

The single cylinder case studied by Cala *et al.*, 1996 is a cylinder without pendulum movement, attached to the lower wall. For this case, experimental results of transversal and vertical velocity and respective fluctuations are available. Here, the cylinder has 75 mm of height and diameter of 19 mm. The inlet boundary condition is the velocity profile measured by Cala *et al.*, 1996. This profile was approximated by a $1/6$ exponencial function, given by:

$$\frac{u}{u_0} = 1,089\left(\frac{z}{H}\right)^{\frac{1}{6}} \tag{36}$$

u_0 is the non-disturbed flow and H is the cylinder height. Figure 1 shows the unstructured mesh used. There is a refinement at the surroundings of the cylinder and immediate downstream of the domain. The mesh has this topology in order to capture all the phenomena that occur at the wake behind the cylinder, and filter any numerical inconsistency downstream. Here, the mesh has 97813 nodes, 538989 elements and 3960 prismatic elements. All the simulations of the present work are transient with time step of 10^{-4} seconds with a total time of 100 seconds. The initial conditions are zero value of all the variables. The convergence criterion is set as 10^{-4} in RMS value of all fields norm.

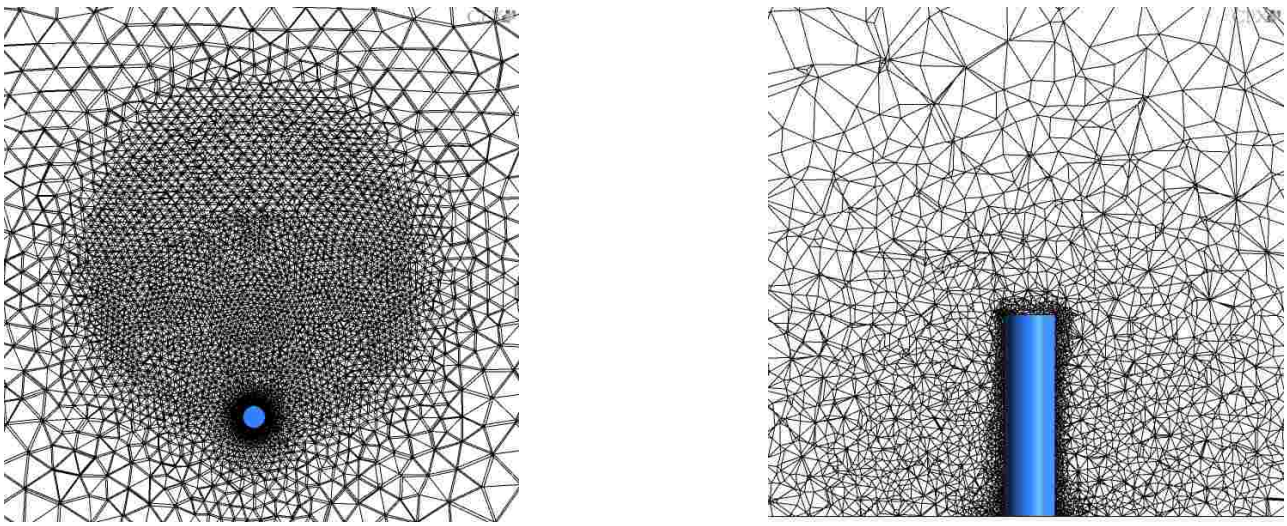

Figure 1: Cylinder mesh

4. Results and Discussion

Figures 2, 3, 4, 5, shows the obtained averaged results. The flow around a circular cylinder holds great engineering interest due to the combined effect of vortex shedding, Kelvin-Helmholtz instabilities and free end flow. Due to that a lot of open issues are shown at the literature. The streamlines show the inherent complexity of that flow. The boundary layer over the finite cylinder is far more complex than the infinite cylinder case. At the 2-Dimensional case, there is a vortex shedding which happens in a characteristic frequency. The length scale varies proportionally with $l^{1/2}$. For the finite cylinder case, the wake topology stands in the way of vortex shedding for cylinders who have low aspect ratio (Kawamura *et al.*, 1984). This occurs due to the strength of tip and necklace vortices who overcome the Kàrman vortices generated between the tip and the junction. The averaged results present at the figures do not show any kind of vortex shedding. The downward motion of the streamlines behind the cylinder junction is followed by the strong upward motion and further downstream (Figure 2). The streamlines located near the bottom wall has a tendency of downward velocity near the stagnation points toward the junction of the cylinder and the bottom wall. This trend results in the downdraft near the cylinder junction (Figure 3). Those visualizations also show the separation of the flow at the top of the cylinder, which agrees with the work of Roh and Park, 2003. The experimental result of Cala, 1996 show, near the plate, a peak of the velocity fluctuation spectra. This can indicate a vortex shedding at that specific point, with a characteristic frequency. At the top of the cylinder, the flow presents itself as unorganized. The appearance of vortex shedding and Von Kárman wakes is governed by the aspect ratio of the cylinder. Eventually, this kind of vorticity appears at the bottom of the cylinder. The flow moves upward and accelerates near the free end, to separate from the cylinder circumference at the free end. At the central wake, the separated shear layer is declined, showing the same effect observed by Park and Lee, 2000. The URANS result show a small recirculation zone, when the LES result show a bigger recirculation zone when compared with the other results. The DES result show small ribbon structures, where the URANS result show a ribbon structure close to the halfway of the cylinder. The LES result has its ribbon structure more attached to the free end. According to Frohlich and Rudi, 2004, this ribbon structure comes as a consequence of the free end vorticity. It can leave the main vortex and stretch downstream in spiralled movement. This effect is observed for the three results, where the LES result show a more spiralled movement.

Figures 3, 4 shows surface streamlines place at the surface of the cylinder. The main objective of this visualizations is to show evidence of tip vortices that separate from the free end and reach down to the wake. It can be seen for the three cases the stagnation lines at the rear of the cylinder and at the oblique left. Close to the bottom of the cylinder, at the oblique stagnation line there is the occurring of a saddle point, which indicates the oncoming of the boundary layer. Close to the free end, there is a point which is a starting point for several streamlines. The LES and DES results shows this points at the same place, and the URANS result shows this place close to the half of the cylinder. Along the stagnation line it can be seen a upward motion, more evident at the URANS result. The LES and DES results shows more homogeneous upward movement. The vertical and horizontal profiles taken at distances of 2D, 4D and 6D are presented at figures 6, 7, 8, 9, 10 and 11. The graphical analysis show that the similar behavior of the profiles downstream of the flow is not observed to regions close to the cylinder in the transversal and vertical profiles. At 2D, for both transversal and vertical profiles, the profile has a different pattern if compared with the other profiles. The tridimensional structure of the flow induces a growth of the velocity close to its symmetry line. This behavior was observed by Cala, 1996, and the author interpreted the mentioned result as a recuperation of the velocity behind the recirculation zone. The numerical results of transversal profiles at 4D and 6D denotes inflexions at points far from the cylinder, disagreeing with the experimental results. Only at 6D, the LES result did not show the inflexion. Those inflexions are an indication of the underestimation of the transversal phenomena from the numerical results. At 2D, all the numerical results had predicted the peak at the fluctuation profile, observed at 1,5R, differently than the experimental results. According to Cala, 1996, this is the limit where the vortex structure produces an important generation rate of turbulent kinetic energy. But the shape of the profile were predicted differently by each numerical result. The LES and DES results were more accurate previewing the shape of the profile, where the URANS results predict a narrower profile. The vertical profiles show the wake form, which shows the recuperation of the kinetic energy downstream where slowly, the level of turbulent intensity diminishes downstream. All the numerical results had shown limited results in predicting those profiles. The worst case happens at 4D, where only the DES result is close to experimental result. This can be as a effects of necklace vortex at the free end and horseshoe vortex at the ground. Numerically, that kind of structure holds great difficulty in prediction due to its small length scale, which requires a even more refined grid to capture those phenomena.

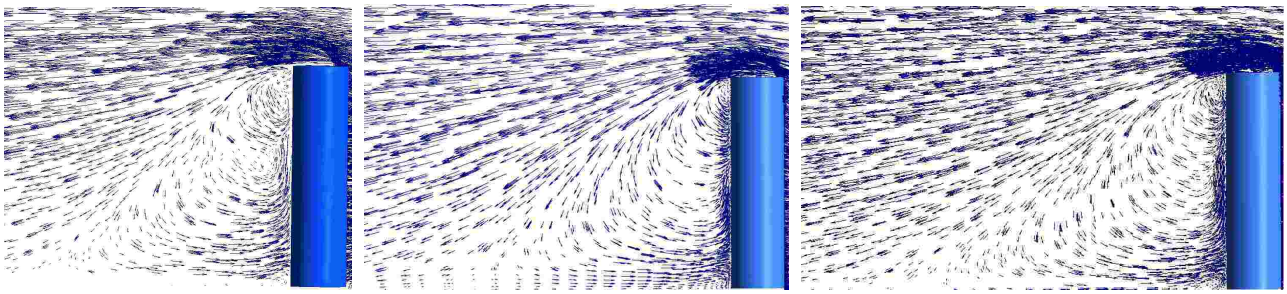

Figure 2: Velocity vectors - From left to right - URANS, DES and LES

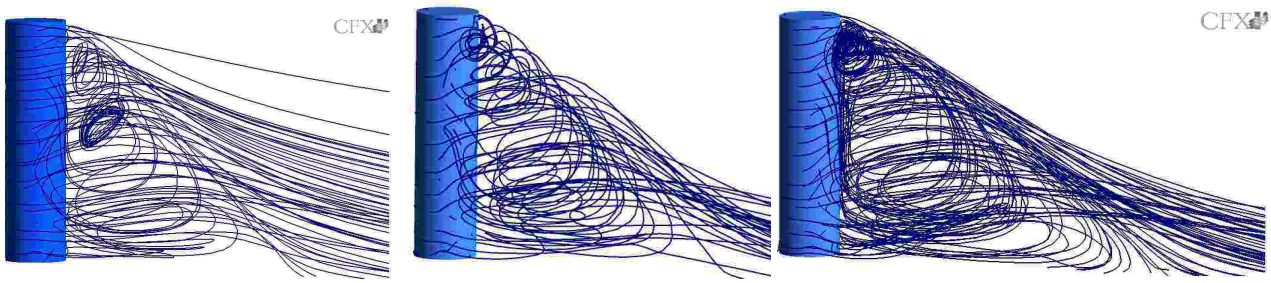

Figure 3: Streamlines - From left to right - URANS, DES and LES

Figure 4: Surface streamlines at rear view of the cylinder - From left to right - URANS, DES and LES

Figure 5: Surface streamlines at a left oblique view of the cylinder - From left to right - URANS, DES and LES

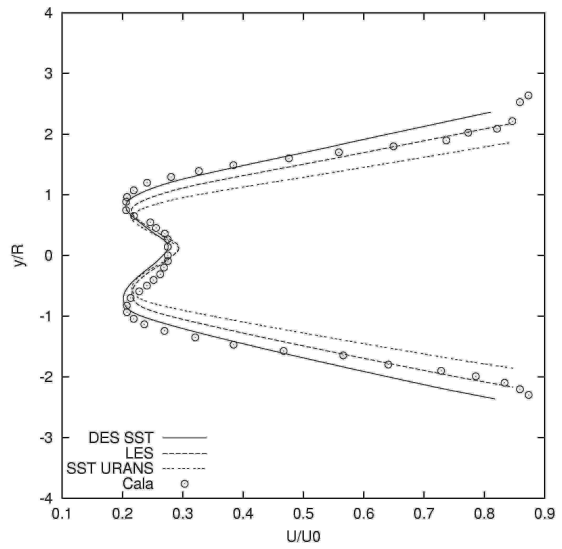

Figure 6: X=2D - Transversal Profile

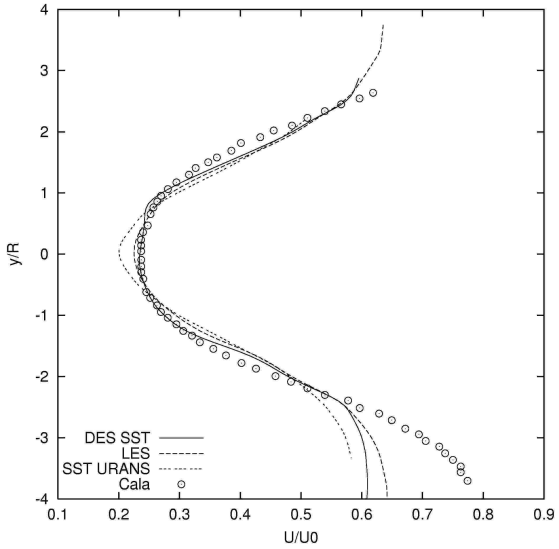

Figure 7: X=4D - Transversal Profile

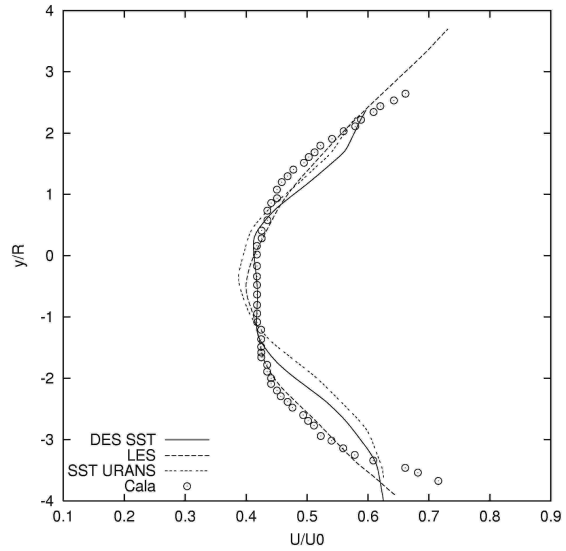

Figure 8: X=6D - Transversal Profile

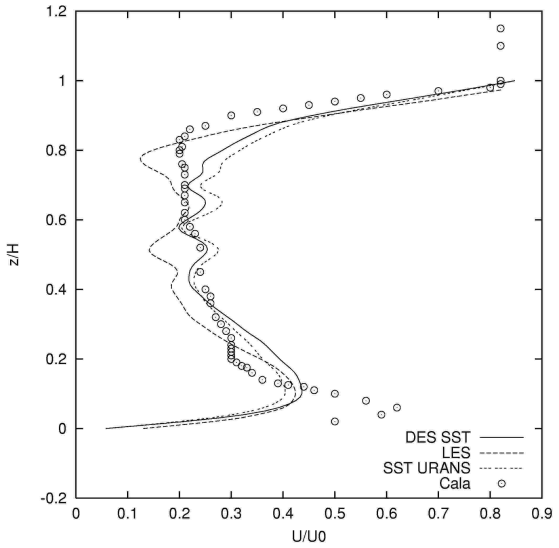

Figure 9: X=2D - Vertical Profile

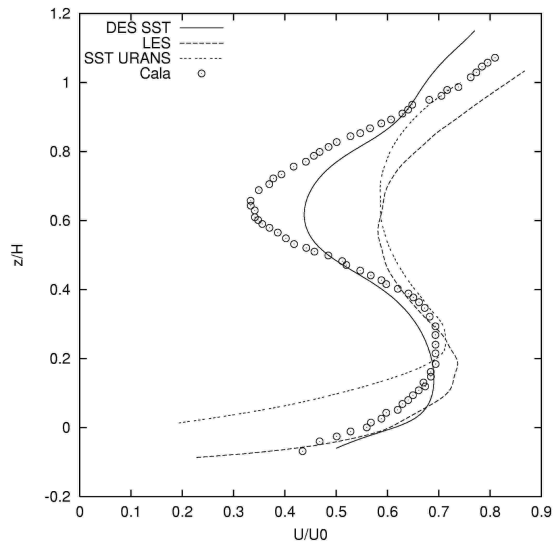

Figure 10: X=4D - Vertical Profile

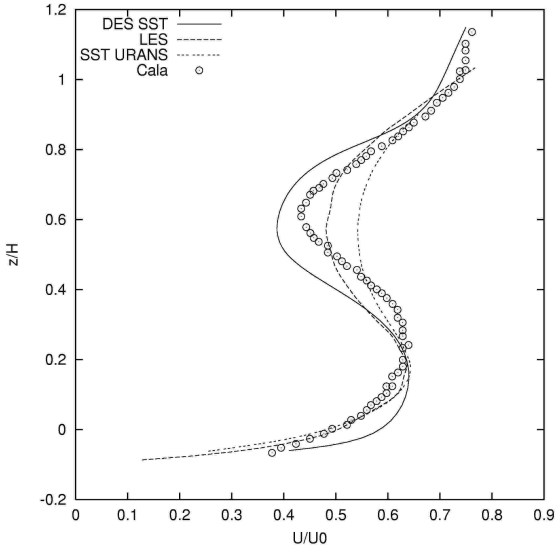

Figure 11: X=6D - Vertical Profile

5. Conclusion

Results of a numerical simulation over a finite cylinder mounted at a flat plate were made. The results are presented at velocity vectors, streamlines at its wake, surface streamlines and graphical validation, where the numerical data obtained by large eddy simulation, detached eddy simulation and URANS is compared to experimental data.

The velocity vectors and streamline display show the behavior of the wake of this kind of flow, where a von Kàrman vortex shedding is expected in theory. The effects that suppress the shedding were visualized. There is also flow separation at the free end of the cylinder, which agrees with experimentation. The surface streamlines at the cylinder shows stagnation line at its rear and close to end at a left oblique view. There are also saddle points which denote the oncoming of boundary layer. The graphical analysis shows that the numerical results have resemblance with experimental result, but the vertical profiles denoted differences when compared with experimentation.

Based on the results, the three models were able to predict fairly the flow. For a more profound analysis, other URANS models should be used. Besides that, for LES analysis, a comparing with different values of the Smagorinsky constant can be done in order to see how the Smagorinsky subgrid model is accurate for this flow. The DES model can also has a similar comparing, with different turbulence models. As a future work, turbulent intensity profiles, spectrum analysis and a analysis of the instantaneous flow will be made in order to make a thorough analysis of the transient result.

6. References

Baban, F., So, R., and Otugen, M., 1989, Unsteady Forces on circular cylinders in a cross-flow, “Experiments in Fluids”, Vol. 7, pp. 293–302.

Cala, C., Brasil-Junior, A. C. P., and Sousa, A. J., 1996, Escoamento Turbulento em Torno de um Cilindro Pendular, “Proceedings of VI ENCIT - Brazilian Congress of Thermal Sciences and Engineering”, Florianópolis, Brazil.

Cala, C. E. C., 1996, Estudo do Escoamento Turbulento Dentro e Sobre uma Matriz de Cilindros Pendulares, Master’s thesis, Universidade de Brasília, DM-018.

Constantinescu, G. S. and Squires, K. D., 2003, LES and DES Investigations of Turbulent Flow over a Sphere at Re=10,000, “Flow, Turbulence and Combustion”, Vol. Vol. 70, pp. pp. 267–298.

Forsythe, J. R., Squires, K. D., and Spalart, P. R., 2001, Detached Eddy Simulation of the Separated Flow over a Forebody Cross Section, B. J. Geurtz, R. F. and Metais, O., editors, “Direct and Large Eddy Simulation IV”, Vol. 8 of “ERCOFTAC Series”, pp. 481–500.

Frohlich, J. and Rudi, W., 2004, LES of the flow around a circular cylinder of finite height, “International Journal of Heat and Fluid Flow”, Vol. 25, pp. 537–548.

Kanda, M., Moriwaki, R., and Kasamatsu, F., 2004, Large Eddy Simulation of Turbulent Organized Structures Within and Above Explicitly Resolved Cube Arrays, “Boundary-Layer Meteorology”, Vol. 112, pp. 343–368.

Kawamura, T., Hiwada, M., Hibino, T., Mabuchi, I., and Kumada, M., 1984, Flow around a finite circular cylinder on a flat plate, “Bull JSME 27:2142-2151”.

Lesieur, M. and Métais, O., 1996, New Trends in Large Eddy Simulation of Turbulence, "Annual Reviews of Fluid Mechanics", Vol. 28, pp. 45–82.

Menter, F. R. and Kuntz, M., 2003, Development and application of a zonal DES turbulence model for CFX 5, Ansys cfx validation report.

Noleto, L. G. and Brasil-Junior, A. C. P., 2005, DES Simulation of a Finite Cylinder Mounted on a Flat Plate, "Proceedings of 18th COBEM - 18th International Congress of Mechanical Engineering", Ouro Preto, Brazil.

Park, C. and Lee, S., 2000, Free end effects on the near wake flow structure behind a finite circular cylinder, "Journal of Wind Engineering and Industrial Aerodynamics", Vol. 88, pp. 231–246.

Roh, S. and Park, S., 2003, Vortical flow over the free end surface of a finite circular cylinder mounted on a flat plate, "Experiments in Fluids", Vol. 34, pp. 63–67.

Rudman, M. and Blackburn, H. M., 1999, Large Eddy Simulation of Turbulent Pipe Flow, "Second International Conference on CFD in Minerals and Process Industries".

Silveira-Neto, A., 2002, Simulação de Grandes Escalas de Escoamentos Turbulentos, Freire, A. P. S., Menut, P., and Su, J., editors, "Turbulência", Vol. 1, pp. 157–188. ABCM.

Silvestrini, J. H., 2003, Simulação Numérica Direta e de Grandes Escalas de Escoamentos Transicionais e Turbulentos, Silveira-Neto, A. and Mansur, S. S., editors, "Turbulência", Vol. 2, pp. 1–72. ABCM.

Spalart, P. R., 2000, Strategies for Turbulence Modelling and Simulation, "International Journal of Heat and Fluid Flow", Vol. 21, pp. 252–263.

Squires, K. D., Forsythe, J. R., Morton, S. A., Strang, W. Z., Wurtzler, K. E., Tomaro, R. F., Grismer, M. J., and Spalart, P. R., January 2002, Progress of Detached Eddy Simulation of Massively Separated Flows, "AIAA 2002-1021".

Strelets, M., 2001, Detached Eddy Simulation of massively Separated Flows, "AIAA 2001-0879".